

GW170817 4.5 YEARS AFTER MERGER: DYNAMICAL EJECTA AFTERGLOW CONSTRAINTS

ARVIND BALASUBRAMANIAN¹, ALESSANDRA CORSI¹, KUNAL P. MOOLEY², KENTA HOTOKEZAKA³, DAVID L. KAPLAN⁴,
DALE A. FRAIL⁵, GREGG HALLINAN², DAVIDE LAZZATI⁶, AND ERIC J. MURPHY⁷

Draft version October 13, 2022

ABSTRACT

GW170817 is the first binary neutron star (NS) merger detected in gravitational waves (GWs) and photons, and so far remains the only GW event of its class with a definitive electromagnetic (EM) counterpart. Radio emission from the structured jet associated with GW170817 has faded below the sensitivity achievable via deep radio observations with the most sensitive radio arrays currently in operation. Hence, we now have the opportunity to probe the radio re-brightening that some models predict, should emerge at late times from the interaction of the dynamically-stripped merger ejecta with the interstellar medium. Here we present the latest results from our deep radio observations of the GW170817 field with the Karl G. Jansky Very Large Array (VLA), 4.5 years after the merger. Our new data at 3 GHz do not show any compelling evidence for emission in excess to the tail of the jet afterglow ($< 3.3 \mu\text{Jy}$), confirming our previous results. We thus set new constraints on the dynamical ejecta afterglow models. These constraints favor single-speed ejecta with energy $\lesssim 10^{50}$ erg (for an ejecta speed of $\beta_0 = 0.5$), or steeper energy-speed distributions of the kilonova ejecta. Our results also suggest larger values of the cold, non-rotating maximum NS mass in equal mass scenarios. However, without a detection of the dynamical ejecta afterglow, obtaining precise constraints on the NS equation of state remains challenging.

Subject headings: GW170817, Kilonova afterglow: general — radio continuum: general

1. INTRODUCTION

GW170817 remains the first and only example yet of the merger of two neutron stars (NSs), observed by LIGO and VIRGO (Abbott et al. 2017b), whose discovery in gravitational waves (GWs) was followed by the identification of a definitive electromagnetic (EM) counterpart from radio to γ -ray frequencies.

The treasure trove of information that this event has provided to the astronomy community cannot be understated. We refer the reader to the many papers written on this event for a comprehensive description of all of the observations that enabled the identification of a coincident gamma-ray burst (GRB; e.g. Abbott et al. 2017a, and references therein); a host galaxy at 40 Mpc and a UV/optical/IR kilonova (e.g., Arcavi et al. 2017; Chornock et al. 2017; Coulter et al. 2017; Cowperthwaite et al. 2017; Drout et al. 2017; Kasliwal et al. 2017; Kasen et al. 2017; Kilpatrick et al. 2017; Pian et al. 2017; Shappee et al. 2017; Smartt et al. 2017; Tanvir et al. 2017; Valenti et al. 2017; Metzger 2017); a delayed non-thermal afterglow observed from radio to X-rays (e.g., Troja et al.

2017; Haggard et al. 2017; Margutti et al. 2017; Hallinan et al. 2017).

Extensive observations of the quasi-thermal kilonova and of the non-thermal afterglow associated with GW170817 have painted a detailed picture of the ejecta that resulted from the merger of the two NSs in the compact binary progenitor of GW170817. While the kilonova was powered by quasi-isotropic and relatively slow neutron-rich debris originating from a combination of dynamical ejecta and disk winds (e.g. Metzger 2017), the non-thermal radio afterglow probed the existence of an off-axis jet that successfully burrowed through the neutron-rich debris. Radio observations, in particular, were instrumental in narrowing down the morphology of relativistic ejecta to a structured jet (a.k.a. jet+cocoon), and in providing crucial insights into the geometry of the merger itself, and the density of the interstellar medium (ISM) through which the jet was launched (Mooley et al. 2018c; Lazzati et al. 2018; Ren et al. 2020; Ghirlanda et al. 2019; Corsi et al. 2018; Dobie et al. 2018; Alexander et al. 2017; Margutti et al. 2018; Mooley et al. 2018a,b; Hajela et al. 2019).

Well before the discovery of GW170817, models had been proposed predicting that, regardless of whether a jet is successfully launched in a binary NS merger, the interaction of the kilonova ejecta with the ISM can produce non-thermal emission in the radio a few years after merger (e.g., Nakar & Piran 2011; Piran et al. 2013; Hotokezaka & Piran 2015), motivating several related observational efforts in cosmological short GRBs (e.g. Metzger & Bower 2014; Fong et al. 2016; Horesh et al. 2016). With GW170817, these late-time re-brightening models have spurred new interest in the community (Kathirgamaraju et al. 2019; Hotokezaka et al. 2018; Bartos et al. 2019; Margalit & Piran 2020; Liu et al. 2020), especially

¹ Department of Physics and Astronomy, Texas Tech University, Box 1051, Lubbock, TX 79409-1051, USA; e-mail: arvind.balasubramanian@ttu.edu

² Caltech, 1200 E. California Blvd. MC 249-17, Pasadena, CA 91125, USA

³ Research Center for the Early Universe, Graduate School of Science, University of Tokyo, Bunkyo-ku, Tokyo 113-0033, Japan

⁴ Center for Gravitation, Cosmology, and Astrophysics, Dept. of Physics, University of Wisconsin-Milwaukee, P.O. Box 413, Milwaukee, WI 53201, USA

⁵ National Radio Astronomy Observatory, Socorro, NM 87801, USA

⁶ Department of Physics, Oregon State University, 301 Weniger Hall, Corvallis, OR 97331, USA

⁷ National Radio Astronomy Observatory, Charlottesville, VA 22903, USA

given their potential to probe the nature of the merger remnant in relation to the Equation of State (EoS) of nuclear matter (see e.g. [Nedora et al. 2021](#), and references therein). Thus, additional observational campaigns have been carried out in search for late-time radio afterglows in both GW170817 ([Balasubramanian et al. 2021](#); [Hajela et al. 2022](#); [Troja et al. 2022](#)) and other short GRBs (e.g., [Klose et al. 2019](#); [Bruni et al. 2021](#); [Grandorf et al. 2021](#); [Ricci et al. 2021](#)), albeit without any definitive detections so far.

Motivated by the above considerations, in [Balasubramanian et al. \(2021\)](#) we presented the deepest radio observations of the GW170817 field at 3.5 years after merger, and found no evidence for a late-time radio re-brightening. This result helped constrain the energy-speed distribution of the kilonova ejecta ([Balasubramanian et al. 2021](#)), and provided hints on the NS EoS ([Nedora et al. 2021](#)). On the other hand, late-time X-ray ob-

servations of the GW170817 field around the same epoch had left open the possibility of late-time emission in excess to that expected from the tail of the GW170817 jet afterglow ([Hajela et al. 2022](#); [Troja et al. 2022](#)). However, continued follow-up in the X-rays at 4.3-4.8 years since merger did not confirm the presence of an X-ray excess at these later times ([Hajela et al. 2021](#); [O’Connor & Troja 2022](#)).

Here, we present new deep observations of the GW170817 field carried out with the Karl G. Jansky Very large Array (VLA) at 3 GHz and at the epoch of about 4.5 years since merger. These observations improve substantially on the sensitivity reached by recently reported radio observations of the same field ([Ricci et al. 2022](#)). Our paper is organized as follows. We report our new observations in §2; in §3 we discuss our results within the kilonova ejecta afterglow model; finally, in §4 we summarize and conclude.

TABLE 1 VLA late-time observations of the GW170817 field. See text for details on RMS measurements.

Date (UT)	ν (GHz)	VLA config.	Time on-source (hr)	RMS (μ Jy)	VLA program	PI	Nominal synth. beam (")
2021 Dec 06	3.0	B	2 h24 m54 s	4.9 (3.6)	21B-057	Balasubramanian	2.1
2021 Dec 20	3.0	B	2 h25 m57 s	4.4 (3.9)	21B-057	Balasubramanian	2.1
2021 Dec 28	3.0	B	2 h25 m57 s	4.7 (3.9)	21B-057	Balasubramanian	2.1
2022 Jan 05	3.0	B	2 h25 m57 s	4.9 (4.3)	21B-057	Balasubramanian	2.1
2022 Mar 05	2.9	A	2 h28 m00 s	4.4 (3.9)	22A-168	Balasubramanian	0.65
2022 Mar 10	3.0	A	2 h28 m08 s	4.4 (3.9)	22A-168	Balasubramanian	0.65
2022 Mar 14	3.0	A	2 h28 m02 s	4.0 (3.9)	22A-168	Balasubramanian	0.65
2022 Mar 17	3.0	A	2 h28 m08 s	4.0 (3.9)	22A-168	Balasubramanian	0.65
2022 Mar 22	3.0	A	2 h28 m10 s	4.1 (4.0)	22A-168	Balasubramanian	0.65
2022 Mar 23	3.0	A	2 h17 m34 s	4.4 (4.1)	22A-168	Balasubramanian	0.65
2022 Mar 28	3.0	A	2 h38 m42 s	3.7 (3.4)	22A-168	Balasubramanian	0.65
2022 Mar 29	3.0	A	2 h28 m00 s	3.9 (3.7)	22A-168	Balasubramanian	0.65

TABLE 2 Results for the co-added late-time radio observations of GW170817. See text for discussion.

Date (UT)	Epoch (yr)	ν (Hz)	F_ν (μ Jy)	σ_ν (μ Jy)	Instrument	Reference
2021 Dec 06 - 2022 Jan 05	4.3	2.8×10^9	< 6.6	2.2	VLA B	This work
2022 Mar 05 - 2022 Mar 29	4.6	3.0×10^9	< 4.5	1.5	VLA A	This work
2021 Dec 06 - 2022 Mar 29	4.5	3.0×10^9	< 3.3	1.1	VLA A&B	This work
2021 Dec 07 - 2022 May 18	4.5	2.41×10^{17}	5.18×10^{-5}	3.44×10^{-5}	Chandra	O’Connor & Troja (2022)

2. OBSERVATIONS AND DATA REDUCTION

We carried out radio continuum observations of the GW170817 field with the VLA. Our observations were executed with the standard VLA S band setup, with a nominal central frequency of 3 GHz, and split in 12 epochs (each providing approximately 2.5 hours on source) between December 2021 and March 2022. The first four epochs were observed with the VLA in its B configuration, while the subsequent eight epochs were carried out with the array in its most extended A configuration. These observations are listed in Table 1. After calibration was performed with the automated VLA calibration pipeline, we manually inspected the data and performed further flagging for radio frequency interference (RFI) as needed. We then imaged the data using the CASA ([McMullin et al. 2007](#)) task `tclean` with one Taylor term (`nterms=1`) and robust weighting (`robust=0.5`;

see also [Balasubramanian et al. 2021](#)), and derived the sensitivity RMS measurements running `imstat` on the residual images within a circular region of radius equal to 10 nominal synthesized beams⁸ around the position of GW170817 ($\alpha = 13\text{h}09\text{m}48.069\text{s}$, $\delta = -23\text{d}22\text{m}53.39\text{s}$, J2000; [Mooley et al. 2018c](#)). Because this region may include residuals associated with the host galaxy light (see Figure 1), we also list in parenthesis in Table 1 the RMS values we obtain using a circular region of the same size in a source-free portion of the image. We find no significant ($> 3 \times \text{RMS}$) excess in a region of one synthesized beam around the position of GW170817 in any of the individual epochs.

Next, we co-add the four B configuration observations, and the eight A configuration observations separately;

⁸ As recommended by [Hancock et al. \(2012\)](#) and [Mooley et al. \(2013\)](#).

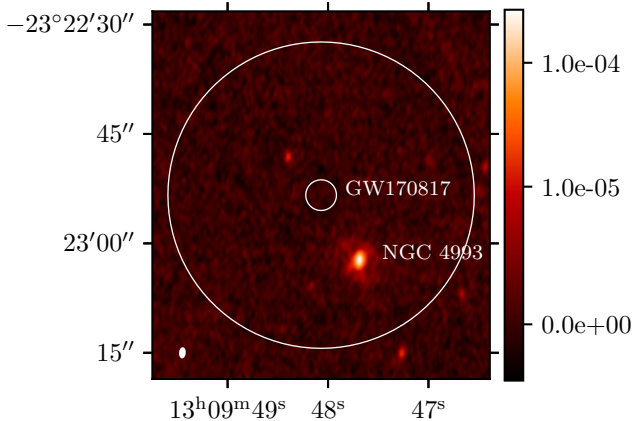


FIG. 1.— Image of the GW170817 field at ≈ 4.5 yrs since merger, as derived from our deepest co-added dataset (see Table 2). The small circle has a radius of $2.1''$ and is centered on the position of GW170817. The larger circle has a radius of $21''$, equal to the radius of the circular region used to calculate our RMS sensitivity in the residual image of the field. The host galaxy of GW170817 is enclosed in this larger circular region. Several sources unrelated to GW170817 are also visible. The synthesized beam ellipse is shown in the bottom left. The color bar gives the flux density in Jy.

finally, we co-add the full multiple configuration data set (all in the visibility domain) for a total of 12 observations. The imaging for these co-added datasets was performed similar to what is described above, with the `CASA` task `tclean` but using `nterms=2` to better clean the emission from bright radio sources in the field. To estimate the RMS sensitivity for the co-added observations in the A and B configurations, we conservatively use a circular region of radius 10 times the nominal synthesized beam width of the B configuration, centered on the location of GW170817 in the residual images (Figure 1 and Table 2). We note that the RMS values estimated this way differ by less than 10% from RMS values calculated in source free regions of the cleaned image. In our deepest co-added image we reach an RMS sensitivity of $1.1 \mu\text{Jy}$ at 3.0 GHz. No emission in excess to $3\times$ the co-added image RMS is found in a circular region of radius 2.1 arcsec (FWHM of the nominal VLA synthesized beam in B configuration at 3 GHz) around the location of GW170817. Specifically, at the location of GW170817 we measure a 3 GHz flux of $2.1 \pm 1.1 \mu\text{Jy}$. Therefore, we constrain the radio emission from GW170817 to $< 3.3 \mu\text{Jy}$ at 4.5 years since merger (see Figure 2).

3. DISCUSSION

In Figure 2, we show the 3 GHz light curve of GW170817 (see the panchromatic afterglow data webpage⁹ for a compilation of the full dataset). The black data points are the previous radio observations (Hallinan et al. 2017; Mooley et al. 2018a,b; Makhathini et al. 2021) that follow the jet+cocoon afterglow model (black line with gray 1σ error region). The red star shows our previous radio detection at ~ 3.5 years since merger (Balasubramanian et al. 2021). The radio upper limit from this work is shown with a downward pointing red triangle. As evident from this Figure, we do not find any significant

evidence for emission in excess to the expectations from a decaying jet+cocoon afterglow model, confirming our previous results (Balasubramanian et al. 2021).

For comparison, in Figure 2 we also show the X-ray flux measurements derived from *Chandra* observations of the GW170817 field are shown as purple squares (see e.g. Haggard et al. 2017; Margutti et al. 2017; Troja et al. 2017; Hajela et al. 2022; Troja et al. 2022, and references therein) extrapolated to the radio band using a radio-to-X-ray spectral index of $\beta = -0.584$ (see Makhathini et al. 2021). Recently, O’Connor & Troja (2022) also reported a measurement of $\sim 0.6 \times 10^{15} \text{ erg cm}^{-2} \text{ s}^{-1}$ for the 0.3 – 10 keV flux of GW170817 at ≈ 4.8 years after the merger (assuming a spectral index of -0.585), using observations carried out with the *Chandra* observatory (O’Connor & Troja 2022; Hajela et al. 2021). We convert this flux into a flux density at 1 keV (see Table 2) and, by combining it with the radio upper-limit presented here, we derive a radio-to-X-ray spectral index of $\beta \gtrsim -0.608$. This is compatible with the best fit value obtained via previous observations of the structured jet afterglow ($\beta = -0.584 \pm 0.002$; Makhathini et al. 2021), and with the results of our analysis at 3.5 years after merger ($\beta = -0.535 \pm 0.024$; Balasubramanian et al. 2021).

Hereafter we discuss the implications of our latest radio observations in the context of the kilonova ejecta model, following the formulation of Kathirgamaraju et al. (2019). In this model, the kilonova blast wave drives a shock through the ISM, resulting in synchrotron emission. Electrons are accelerated to a power-law distribution of Lorentz gamma factors $\gamma_e > \gamma_{e,m}$, with power-law index p . The energy in the kilonova spherical blast wave is distributed as $E(> \beta\gamma) \propto (\beta\gamma)^{-\alpha}$ (with γ being the Lorentz factor, β being the speed in units of speed of light of the shocked fluid and α being the power law index of the energy speed distribution) and normalized to the total energy E at some minimum velocity β_0 such that $E(> \beta_0\gamma_0) = E$. It is reasonable to assume that radio (GHz) observations are in between the minimum frequency, ν_m (corresponding to γ_m , see Nakar & Piran 2011), and the cooling frequency, ν_c . In this case, the kilonova peak flux density reads (Nakar & Piran 2011):

$$F_{\nu,\text{pk}} \approx (1.5 \text{ mJy}) \epsilon_{e,-1}^{p-1} \epsilon_{B,-3}^{\frac{p+1}{4}} n_{-2}^{\frac{p+1}{4}} \beta_0^{\frac{5p-7}{2}} E_{51} \nu_{9.5}^{\frac{1-p}{2}} d_{26}^{-2}, \quad (1)$$

where $Q_x = Q/10^x$ is followed for all quantities (Q , all expressed in cgs units); ϵ_B and ϵ_e are the fractions of the total energy in the magnetic field and electrons respectively; n , the number density of the medium; d is the distance to the source; the normalization constant is calculated for $p = 2.1$. The time at which the kilonova afterglow emission peaks can be calculated as (Kathirgamaraju et al. 2019):

$$t_{\text{dec}} = t_{\text{pk}} \approx (3.3 \text{ yr}) \left(\frac{E_{51}}{n_{-2}} \right)^{\frac{1}{3}} \beta_0^{-\frac{2}{3}} \left(\frac{2 + \alpha}{\beta_0(5 + \alpha)} - 1 \right). \quad (2)$$

where α is the power law index of the energy speed distribution discussed earlier. The blast wave can be approximated to be mildly relativistic before this peak, and therefore the rising part of the kilonova ejecta light curve

⁹ http://www.tauceti.caltech.edu/kunal/gw170817/gw170817_afterglow_data_full.txt and <https://github.com/kmooley/GW170817/>

can be easily modeled as (see [Kathirgamaraju et al. 2019](#), and references therein):

$$F_{\nu, \text{KN}}(t) = F_{\nu, \text{pk}} \left(\frac{t}{t_p} \right)^s, \quad (3)$$

where:

$$s = \frac{3\alpha - 6(p - 1)}{8 + \alpha}. \quad (4)$$

For $\alpha = \infty$, Equations (1)-(3) reduce to the case of a spherical outflow of total energy E with uniform velocity β_0 ([Nakar & Piran 2011](#)). In this case, our flux upper-limit at 4.5 yr constrains the energy E and speed β_0 for a given choice of the density and micro-physical parameters. Indeed, setting these parameters as in [Makhathini et al. \(2021\)](#), an energy of $E \approx 10^{50}$ erg and speed of $\beta_0 \approx 0.5$ would produce a radio peak flux comparable to our 3σ upper-limit at 4.5 yrs since merger. Hence, single-speed ejecta more energetic than $E \approx 10^{50}$ erg must be slower than $\beta_0 \approx 0.5$. Else, radio emission from such ejecta would have peaked before 4.5 yrs in the radio, at a flux level above $3.3 \mu\text{Jy}$.

Next, in [Figure 3](#) we consider the case of a stratified ejecta with an energy-speed distribution described by the parameter $\alpha < \infty$. In this case, we can use our observations to constrain the values of α under specific assumptions on the energy and minimum speed of the ejecta, and of the density and micro-physical parameters. The blue and green curves in the left panel of [Figure 3](#) show the rising portion of the predicted kilonova afterglow. Specifically, the shades of solid blue curves assume the parameters $E = 10^{51}$ erg, $\beta_0 = 0.3$, $p = 2.1$, $\epsilon_e = 7.8 \times 10^{-3}$, $\epsilon_B = 9.9 \times 10^{-4}$, $n = 9.8 \times 10^{-3} \text{cm}^{-3}$, $d = 40$ Mpc (as in [Makhathini et al. 2021](#)); the dotted green and red curves assume the parameters $E = 10^{51}$ erg, $\beta_0 = 0.3$, $p = 2.2$, $\epsilon_e = 10^{-1}$, $\epsilon_B = 10^{-3}$, $n = 10^{-2} \text{cm}^{-3}$, $d = 40$ Mpc (as in [Kathirgamaraju et al. 2019](#)). The radio observations presented here (red downward pointing triangle for our 3σ upper-limit) constrain α to $\alpha \gtrsim 6$ if we assume the parameters as in [Makhathini et al. \(2021\)](#). This is compatible with the constraints one can derive from the X-ray observations reported by [O'Connor & Troja \(2022\)](#) within the large error bars that affect this X-ray measurement (see the last purple square in [Figure 3](#)). For the more general choice of micro-physical parameters ([Kathirgamaraju et al. 2019](#)), our latest upper-limit is compatible only with the more extreme cases of very steep values of α or with a kilonova blast wave comprised of a single velocity component ($\alpha = \infty$).

The results presented here can also improve on the constraints discussed in [Nedora et al. \(2021\)](#) regarding the NS EoS. In the right panel of [Figure 3](#) we show a plot of the EoS-dependent model radio light curves from [Nedora et al. \(2021\)](#), compared with the radio upper-limit derived in this analysis. As evident from this [Figure](#), our radio observations at 4.5 yrs since merger add new constraints on the possible EoSs, disfavoring the softer EoS SFHo (with $p = 2.05$, $\epsilon_e = 0.1$, $\epsilon_B = 0.01 - 0.001$ and $n = (4 - 5) \times 10^{-3} \text{cm}^{-3}$), as well as the stiffer

LS220 (with $p = 2.05$, $\epsilon_e = 0.1$, $\epsilon_B = 0.01 - 0.001$ and $n = 5 \times 10^{-3} \text{cm}^{-3}$) in moderate mass ratio scenarios ($q \lesssim 1.43$). The SFHo and LS220 EoSs predict the same maximum mass of the cold non-rotating NS, but LS220 correlates with a steeper ejecta energy-speed distribution for $q = 1$ ([Radice et al. 2018](#)). On the other hand, scenarios like a DD2 EoS with $q = 1$, that predict a larger value of the cold, non-rotating maximum NS mass, are still possible.

4. SUMMARY AND CONCLUSION

In this work, we have presented deep, 3 GHz observations of GW170817 at ≈ 4.5 years since merger. We co-added all the data collected with the VLA via our programs to obtain a deep image of the field, and find no evidence for a re-brightening that can be associated with the kilonova ejecta afterglow in the radio. This confirms our previous results ([Balasubramanian et al. 2021](#)). Overall, the upper-limit we set here and the latest X-ray observations reported by [O'Connor & Troja \(2022\)](#) reinforce the conclusion that there is no clear evidence for a late-time re-brightening of the GW170817 non-thermal afterglow emission. Qualitatively speaking, models that envision the emergence of a new emission component at late times, with constant or declining X-ray emission beyond the epoch of ≈ 3.5 yrs since merger and without accompanying bright radio emission, could likely still be fit to the data ([Hajela et al. 2022](#)) but would be very hard to test via further radio (or X-ray) observations of the GW170817 field.

Kilonova ejecta afterglow models could still be constrained with further radio observations of sensitivity similar to the one reached in this work (and thus not without a substantial investment of observing time). Indeed, the observations presented here tighten the constraints on the power-law index of the energy-speed distribution of the kilonova ejecta to $\alpha \gtrsim 6$, somewhat steeper than the $\alpha \gtrsim 5$ constraint that we obtained at 3.5 years post-merger (see [Balasubramanian et al. 2021](#)), and favor EoS predicting larger values of the cold, non-rotating NS mass for $q = 1$ scenarios.

In the future, a radio non-detection at 7.5 yrs since merger would constrain the ejecta energy-speed distribution to $\alpha \gtrsim 10$ for reasonable assumptions on the ejecta parameters. A detection would also facilitate more precise constraints on the possible EoSs (see e.g. BLh in the right panel of [Figure 3](#)), though previous considerations regarding the challenges of pinpointing a specific EoS remain true (see e.g. [Nedora et al. 2021](#); [Balasubramanian et al. 2021](#)).

A.B. and A.C. acknowledge support from NSF AST-1907975. K.P.M. and G.H. acknowledge support from the National Science Foundation Grant AST-1911199. D.L. acknowledges support from NSF grant AST-1907955. The National Radio Astronomy Observatory is a facility of the National Science Foundation operated under cooperative agreement by Associated Universities, Inc.

REFERENCES

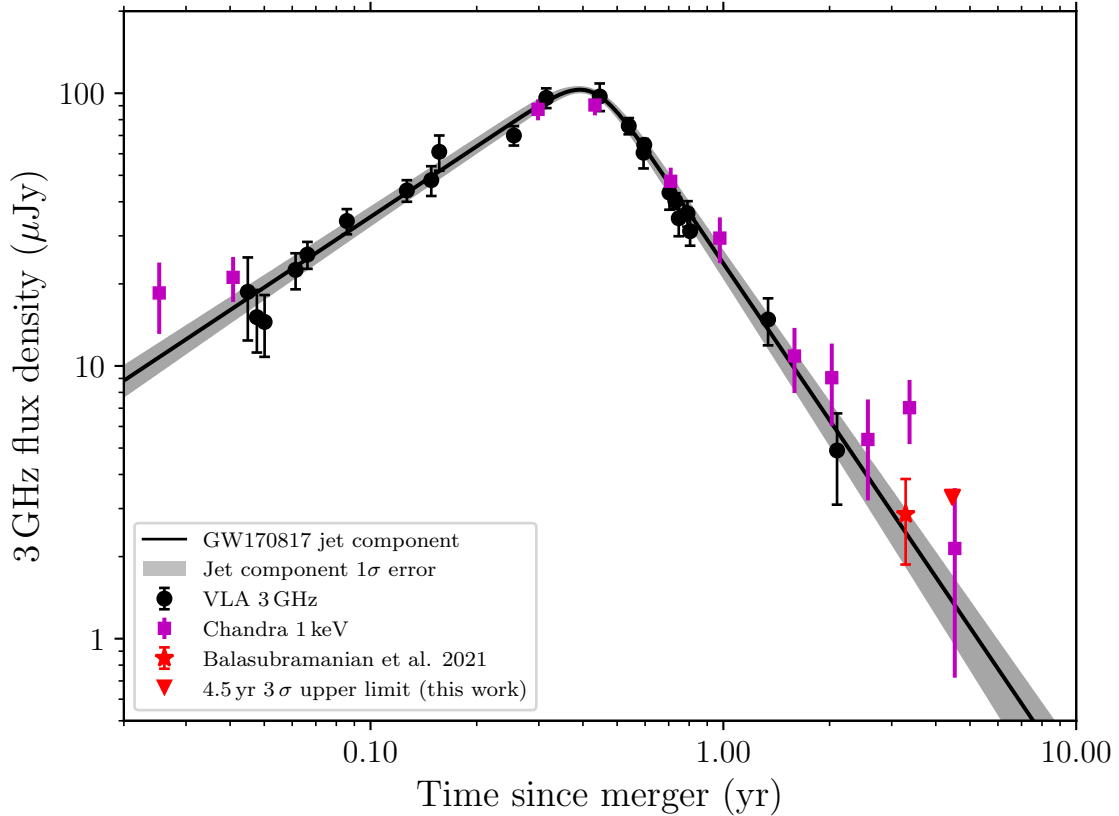


FIG. 2.— 3 GHz radio light curve of GW170817 with the best fit structured jet model from Makhathini et al. (2021). Radio data are shown as black data points. The *Chandra* 1 keV data scaled to 3 GHz with a power-law index of $\beta = -0.584$ (including the latest measurement by O’Connor & Troja 2022, and references therein). We extrapolate all X-ray data to 3 GHz using $\beta = -0.584$ because there is only marginal evidence for a potential spectral flattening around 3.5 yrs since merger (Balasubramanian et al. 2021; Hajela et al. 2022) which, however, has not been confirmed in later observations by O’Connor & Troja (2022). Our previous observation 3.5 years since merger is marked with a red star (Balasubramanian et al. 2021). The 3σ upper limit from this work is shown as red downward pointing triangle.

Arcavi, I., Hosseinzadeh, G., Howell, D. A., et al. 2017, *Nature*, 551, 64
 Balasubramanian, A., Corsi, A., Mooley, K. P., et al. 2021, *ApJ*, 914, L20
 Bartos, I., Lee, K. H., Corsi, A., Márka, Z., & Márka, S. 2019, *MNRAS*, 485, 4150
 Bruni, G., O’Connor, B., Matsumoto, T., et al. 2021, *MNRAS*, 505, L41
 Chornock, R., Berger, E., Kasen, D., et al. 2017, *ApJ*, 848, L19
 Corsi, A., Hallinan, G. W., Lazzati, D., et al. 2018, *ApJ*, 861, L10
 Coulter, D. A., Foley, R. J., Kilpatrick, C. D., et al. 2017, *Science*, 358, 1556
 Cowperthwaite, P. S., Berger, E., Villar, V. A., et al. 2017, *ApJ*, 848, L17
 Dobie, D., Kaplan, D. L., Murphy, T., et al. 2018, *ApJ*, 858, L15
 Drout, M. R., Piro, A. L., Shappee, B. J., et al. 2017, *Science*, 358, 1570
 Fong, W., Metzger, B. D., Berger, E., & Özel, F. 2016, *ApJ*, 831, 141
 Ghirlanda, G., Salafia, O. S., Paragi, Z., et al. 2019, *Science*, 363, 968
 Grandorf, C., McCarty, J., Rajkumar, P., et al. 2021, *ApJ*, 908, 63
 Haggard, D., Nynka, M., Ruan, J. J., et al. 2017, *ApJ*, 848, L25
 Hajela, A., Margutti, R., Alexander, K. D., et al. 2021, *GRB Coordinates Network*, 31231, 1
 —. 2019, *ApJ*, 886, L17
 Hajela, A., Margutti, R., Bright, J. S., et al. 2022, *ApJ*, 927, L17
 Hallinan, G., Corsi, A., Mooley, K. P., et al. 2017, *Science*, 358, 1579
 Hancock, P. J., Murphy, T., Gaensler, B. M., Hopkins, A., & Curran, J. R. 2012, *MNRAS*, 422, 1812
 Horesh, A., Hotokezaka, K., Piran, T., Nakar, E., & Hancock, P. 2016, *ApJ*, 819, L22

Hotokezaka, K., Kiuchi, K., Shibata, M., Nakar, E., & Piran, T. 2018, *ApJ*, 867, 95
 Hotokezaka, K., & Piran, T. 2015, *MNRAS*, 450, 1430
 Kasen, D., Metzger, B., Barnes, J., Quataert, E., & Ramirez-Ruiz, E. 2017, *Nature*, 551, 80
 Kasliwal, M. M., Nakar, E., Singer, L. P., et al. 2017, *Science*, 358, 1559
 Kathirgamaraju, A., Giannios, D., & Beniamini, P. 2019, *MNRAS*, 487, 3914
 Kilpatrick, C. D., Foley, R. J., Kasen, D., et al. 2017, *Science*, 358, 1583
 Klose, S., Nicuesa Guelbenzu, A. M., Michałowski, M. J., et al. 2019, *ApJ*, 887, 206
 Lazzati, D., Perna, R., Morsony, B. J., et al. 2018, *Phys. Rev. Lett.*, 120, 241103
 Liu, L.-D., Gao, H., & Zhang, B. 2020, *ApJ*, 890, 102
 Makhathini, S., Mooley, K. P., Brightman, M., et al. 2021, *ApJ*, 922, 154
 Margalit, B., & Piran, T. 2020, *MNRAS*, 495, 4981
 Margutti, R., Berger, E., Fong, W., et al. 2017, *ApJ*, 848, L20
 Margutti, R., Alexander, K. D., Xie, X., et al. 2018, *ApJ*, 856, L18
 McMullin, J. P., Waters, B., Schiebel, D., Young, W., & Golap, K. 2007, in *Astronomical Society of the Pacific Conference Series*, Vol. 376, *Astronomical Data Analysis Software and Systems XVI*, ed. R. A. Shaw, F. Hill, & D. J. Bell, 127
 Metzger, B. D. 2017, arXiv e-prints, arXiv:1710.05931
 Metzger, B. D., & Bower, G. C. 2014, *MNRAS*, 437, 1821
 Mooley, K. P., Frail, D. A., Ofek, E. O., et al. 2013, *ApJ*, 768, 165
 Mooley, K. P., Nakar, E., Hotokezaka, K., et al. 2018a, *Nature*, 554, 207
 Mooley, K. P., Frail, D. A., Dobie, D., et al. 2018b, *ApJ*, 868, L11
 Mooley, K. P., Deller, A. T., Gottlieb, O., et al. 2018c, *Nature*, 561, 355

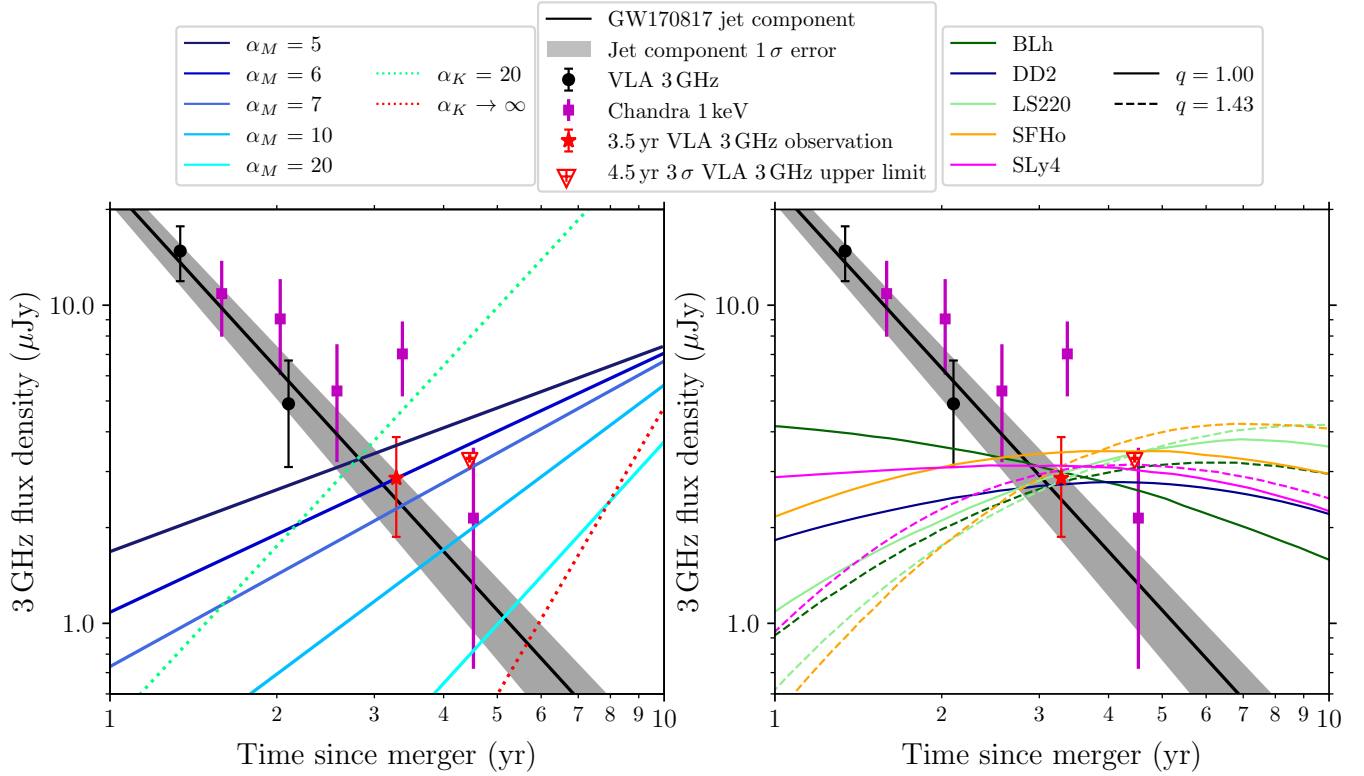


FIG. 3.— Late-time observations of the GW170817 field at 3 GHz from Makhathini et al. (2021) (black dots), Balasubramanian et al. (2021) (red star), and from this work (red downward pointing triangle for our 3σ upper-limit). *Chandra* 1 keV observations scaled to 3 GHz with a power-law index of $\beta = -0.584$ (including the latest measurement by O’Connor & Troja 2022) are shown as purple squares (see e.g. Haggard et al. 2017; Margutti et al. 2017; Troja et al. 2017; Hajela et al. 2022; Troja et al. 2022, and references therein). We extrapolate all X-ray data to 3 GHz using $\beta = -0.584$ because there is only marginal evidence for a potential spectral flattening around 3.5 yrs since merger (Balasubramanian et al. 2021; Hajela et al. 2022) which, however, has not been confirmed in later observations by O’Connor & Troja (2022). We compare these observations with predicted kilonova afterglow light curves. *Left*: The solid lines in various shades of blue are the predicted kilonova afterglow light curves as a function of α (see §3) with the assumption that the minimum speed of the ejecta is $\beta_0 = 0.3$, for the parameters $E = 10^{51}$ erg, $p = 2.1$, $\epsilon_e = 7.8 \times 10^{-3}$, $\epsilon_B = 9.9 \times 10^{-4}$, $n = 9.8 \times 10^{-3} \text{cm}^{-3}$, $d = 40$ Mpc (as in Makhathini et al. 2021) and $\alpha_M = 5, 6, 7, 10, 20$ (subscript M indicates parameters from Makhathini et al. (2021)). For comparison, the green and red dashed line show the case $E = 10^{51}$ erg, $\epsilon_e = 10^{-1}$, $\epsilon_B = 10^{-3}$, $n = 10^{-2} \text{cm}^{-3}$, $p = 2.2$, $d = 40$ Mpc (as in Kathirgamaraju et al. 2019), with $\alpha_K = 20, \infty$ (subscript K indicates parameters from Kathirgamaraju et al. (2019); see §3); *Right*: Predicted radio light curves of BNS ejecta for different EoS and mass ratios reproduced from Nedora et al. (2021) (see their Figure 4 and Table 2). See §3 for discussion.

Nakar, E., & Piran, T. 2011, *Nature*, 478, 82
 Nedora, V., Radice, D., Bernuzzi, S., et al. 2021, *MNRAS*, 506, 5908
 O’Connor, B., & Troja, E. 2022, *GRB Coordinates Network*, 32065, 1
 Pian, E., D’Avanzo, P., Benetti, S., et al. 2017, *Nature*, 551, 67
 Piran, T., Nakar, E., & Rosswog, S. 2013, *MNRAS*, 430, 2121
 Radice, D., Perego, A., Hotokezaka, K., et al. 2018, *ApJ*, 869, 130
 Ren, J., Lin, D.-B., Zhang, L.-L., et al. 2020, *ApJ*, 901, L26
 Ricci, R., O’Connor, B., & Troja, E. 2022, *GRB Coordinates Network*, 32094, 1
 Ricci, R., Troja, E., Bruni, G., et al. 2021, *MNRAS*, 500, 1708

Shappee, B. J., Simon, J. D., Drout, M. R., et al. 2017, *Science*, 358, 1574
 Smartt, S. J., Chen, T. W., Jerkstrand, A., et al. 2017, *Nature*, 551, 75
 Tanvir, N. R., Levan, A. J., González-Fernández, C., et al. 2017, *ApJ*, 848, L27
 Troja, E., Piro, L., van Eerten, H., et al. 2017, *Nature*, 551, 71
 Troja, E., O’Connor, B., Ryan, G., et al. 2022, *MNRAS*, 510, 1902
 Valenti, S., Sand, D. J., Yang, S., et al. 2017, *ApJ*, 848, L24